An Axisymmetric Hybrid Model for the Plasma Transport in a Helicon Plasma Thruster

J. Zhou[1,2], A. Domínguez[1], D. Pérez-Grande[1], P. Fajardo[1] and E. Ahedo[1]

[1]Equipo de Propulsión Espacial y Plasmas, Universidad Carlos III de Madrid, 28911 Leganés, Spain, Email[2]: jzhou@pa.uc3m.es

KEYWORDS:

Helicon plasma thruster, hybrid codes, magnetic field aligned meshes

ABSTRACT:

The plasma discharge inside a Helicon Plasma Thruster (HPT) chamber is studied. A preliminary version of a novel two-dimensional asymmetric code under development for HPT is used for the analysis. The dynamics of the plasma is described with a hybrid approach: a particle-in-cell method for the heavy species and a fluid model for electrons. Regarding the plasma-wave interaction it is not simulated for now and a known map of the energy given to the plasma is assumed. Results such as electric potential, plasma density, neutral depletion, electron streamlines and so on from a simulation case are presented and discussed.

1. INTRODUCTION

The Helicon Plasma Thruster (HPT) is still an experimental technology and it is being researched extensively at present [1–6]. The main physical processes of its operation are not fully understood yet. The plasma discharge in an HPT has two distinguished parts: (i) the plasma production and heating processes, achieved via the electron interaction with the helicon waves emitted by the device antenna, and (ii) the plasma transport inside the thruster chamber and in the external magnetic nozzle. Regarding the plasma-wave interaction the main mechanism causing the heating remains unclear. Most theoretical models adopt collisional models on a cold plasma, but there are certain evidences showing that the main mechanism could be another [7–9]. As to the plasma transport, there are discrepancies between the optimistic capabilities predicted by existing models and the meager performances of the experiments [5, 6].

This work reports on the progresses on a 2D code aiming to advance on the understanding on HPT physics and propulsive performances. Once completed the code will be used to optimize the design of HPT-05 prototype, a 1kW-class HPT being developed by our research group EP2 and SENER [10] and tested in EP2 facilities [6].

This HPT code borrows many elements on a similar one being developed by EP2 for Hall Effect Thrusters (HET) and which is in a more advanced state of development [11, 12]. The code takes a two-dimensional axisymmetric approach and has a hybrid concept: a particle-in-cell (PIC) formulation is adopted for the heavy species (ions and neutrals) and a magnetized fluid formulation for electrons. This hybrid formulation is adequate to deal with weakly-collisional plasmas, magnetized electrons and a low plasma-beta. The code under development for HPTs maintain basically the structure of the HET code but introduces changes associated to its different physical principles of operation (energy source, plasma acceleration, magnetic topology...).

The current version of the code is already capable of solving the plasma transport within the chamber, assuming a simple state law for electron thermodynamics (isothermal or polytropic). This simplified problem is similar to the one analyzed previously by Ahedo and Navarro-Cavallé [13]. These authors follow a quasi-2D, fully-fluid approach, with a purely-axial magnetic field inside a cylindrical thruster chamber. Several simplifications on the plasma transport were assumed additionally. These previous results allow us, first, a partial validation of the current hybrid development. Second, we can start freeing some restrictions and simplifications of that model, such as implementing different magnetic topologies, or obtaining a consistent 2D transport of the three plasma species.

2. CODE STRUCTURE

The full structure of the code consists of four independent modules that interact among them: an Ion(I)-module dealing with the transport of heavy species (ions and neutrals); an Electron(E)-module solving for the electron fluid and the electric potential; a Sheath(S)-module solving for the non-neutral sheaths around walls and electrodes; and a Wave(W)-module dealing with the high-frequency plasma-wave interaction. The three first modules are being adapted from the HET-related code [11, 12]. The W-Module is being developed independently [14] and will provide the electron power absorption distribution to be coupled to the electron energy equation in the E-module. At present, the electron energy equation is substituted by a polytropic or isothermal state law for the electron tem-
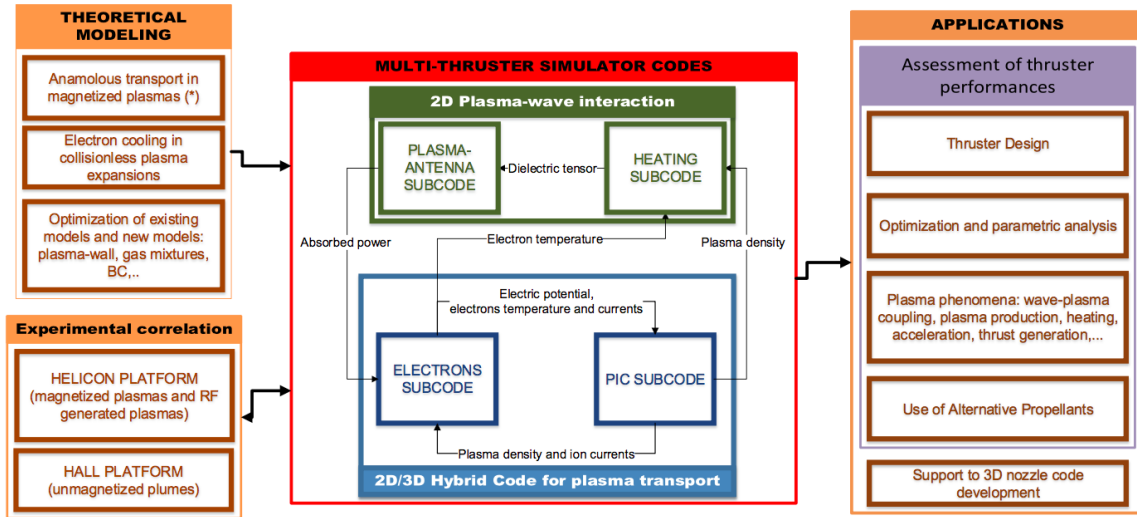
Figure 1: Scheme of the code to developed for HPTs. There is a sheath module together with the electron module inside the box corresponding to the electron subcode.

perature.

The I- and E-modules are run sequentially and both communicate with the S-module to apply the correct conditions at the simulation domain boundaries. The I-module propagates the heavy species to obtain the plasma density and particle fluxes using the electric potential and electron temperature provided by the E-module. Then, the E-module is run to update the electron potential and temperature based on the plasma density and heavy species velocities computed previously by the I-module. The structure of the code with its different modules and their interactions are summarized in Fig. 1.

The main characteristics of the three modules already running are detailed in [11, 12] and are just briefly commented here.

- I-module. It is based on three algorithms to solve the heavy species: a particle collider that carry out the collisions, a particle mover that propagates the trajectories of the particles, and a particle-surface interaction algorithm. The last algorithm includes a kinetic Bohm forcing algorithm to make the ion species fulfill the Bohm condition at the edge of the (quasineutral) simulation domain. Moreover, dedicated computational lists, storing all particle related information, are considered for each ion and neutral species. Besides, a specific particle-list-wise population control algorithm is applied to get an optimum number of particles per cell and reduce the typical noise of a PIC code.

- E-module. Here, magnetized fluid equations are derived by taking moments of the Boltzmann kinetic equation and considering different temperatures in the direction parallel and perpendicular to the magnetic field. Then

a bi-Maxwellian description is assumed for the electron distribution function to close the equations in the fourth order moment of the Boltzmann equation corresponding to heat fluxes. A Finite Volume Method (FVM) is used to solve these fluid equations on a mesh aligned with the magnetic field. The magnetic field aligned mesh allows to reproduce the anisotropy existing for magnetized electrons [15].

- S-module. It provides the plasma response from the interaction with walls and electrodes. As the simulation domain is assumed quasineutral, the sheaths are discontinuities of zero thickness coupling the plasma bulk to the walls. A main result is the sheath potential drop in terms of the plasma wall-perpendicular currents, plasma density and energies.

3. PROBLEM DESCRIPTION

The plasma transport inside a HPT chamber is studied here. The chamber has a cylindrical shape as represented in Fig. 2. The propellant is injected from the back surface and is ionized by bombardment of energetic electrons. The created plasma is contained by cylindrical ceramic walls, and then the plasma jet escapes at the right open end. The plasma is also confined by an externally applied magnetic field. As pointed out previously, the interaction between the rf waves and the electrons is not simulated here. Instead, electrons are assumed here to have a constant, isotropic temperature T_e - which can be understood as an average value-. The electron absorbed power to keep that temperature can be determined as part of the solution.

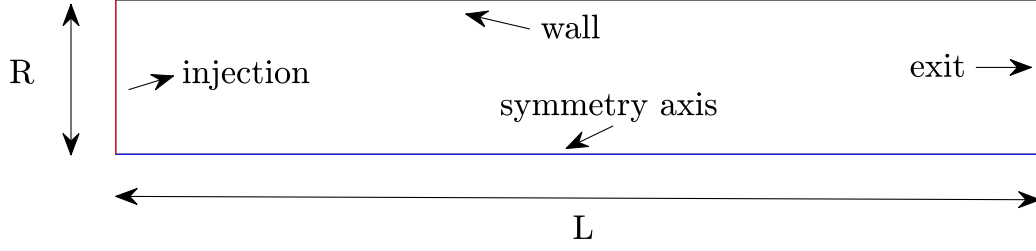The relevant electron particle and momentum

Figure 2: General scheme of the simulation domain. The red line represents the injection surface, the black line the lateral ceramic wall and the green one the exit surface. L is the axial extension of the domain and R its radial extension.

equations are the following [11, 13]:

$$\nabla \cdot (\mathbf{j_e} + \mathbf{j_i}) = 0, \quad \text{(Eq. 1)}$$

$$0 = en\frac{\partial \phi}{\partial \mathbf{l}_\parallel} - T_e\frac{\partial n}{\partial \mathbf{l}_\parallel} - m_e n(\nu_e u_{\parallel e} - \nu_{ei} u_{\parallel i}), \quad \text{(Eq. 2)}$$

$$0 = en\frac{\partial \phi}{\partial \mathbf{l}_\perp} - T_e\frac{\partial n}{\partial \mathbf{l}_\perp} - enBu_{\theta e} - m_e n(\nu_e u_{\perp e} - \nu_{ei} u_{\perp i}),$$
$$\text{(Eq. 3)}$$

$$0 = enBu_{\perp e} - m_e n\nu_e u_{\theta e}. \quad \text{(Eq. 4)}$$

Here: $\mathbf{l}_\parallel$ and $\mathbf{l}_\perp$ are unit vectors parallel and perpendicular (in the meridian plane) to the magnetic field $\mathbf{B}$, respectively; ϕ is the electric potential, n is the density of the quasineutral plasma (with singly-charged ions only), T_e is the electron temperature (constant here); $u_{\perp e}$, $u_{\theta e}$ and $u_{\parallel e}$ are the three electron velocity components, $u_{\perp i}$ and $u_{\parallel i}$ are ion velocity components; $\mathbf{j_e} = -en\mathbf{u_e}$ and $\mathbf{j_i} = en\mathbf{u_i}$ are the electron and ion current densities; $\nu_e = \nu_{en} + \nu_{ei} + \nu_{ion}$ is the total electron collisional frequency, with ν_{ei} the electron-ion collisional frequency, ν_{en} the electron-neutral collisional frequency, and ν_{ion} the ionization frequency.

The three electron momentum equations can be arranged and expressed as generalized Ohm law. After some algebra, the result is

$$j_{\parallel e} = \sigma_\parallel \left(-\frac{\partial \phi}{\partial \mathbf{l}_\parallel} + \frac{T_e}{e}\frac{\partial \ln n}{\partial \mathbf{l}_\parallel} - \frac{m_e \nu_{ei}}{e^2 n}j_{\parallel i} \right), \quad \text{(Eq. 5)}$$

$$j_{\perp e} = \sigma_\perp \left(-\frac{\partial \phi}{\partial \mathbf{l}_\perp} + \frac{T_e}{e}\frac{\partial \ln n}{\partial \mathbf{l}_\perp} - \frac{m_e \nu_{ei}}{e^2 n}j_{\perp i} \right) \quad \text{(Eq. 6)}$$

$$j_{\theta e} = \beta_e j_{\perp e}. \quad \text{(Eq. 7)}$$

Here, the Hall parameter and the conductivities are

$$\beta_e = \frac{\omega_{ce}}{\nu_e}, \quad \sigma_\parallel = \frac{e^2 n}{m_e \nu_e}, \quad \sigma_\perp = \frac{\sigma_\parallel}{1 + \beta_e^2} \quad \text{(Eq. 8)}$$

with $\omega_{ce} = eB/m_e$ the electron gyrofrequency.

Substituting this vector Ohm law into the current conservation equation and having n and $\mathbf{j_i}$ from the I-module, we obtain an elliptic equation for the electric potential file $\phi(z, r)$. For the present case, the

boundary conditions of this problem are zero net current through all the boundary surfaces:

$$\mathbf{j}_e \cdot \mathbf{n}_b = -\mathbf{j}_i \cdot \mathbf{n}_b, \quad \text{(Eq. 9)}$$

where $\mathbf{n}_b$ is an unit vector normal to the boundary surface. The Ohm law shows that this condition on the current becomes a condition on the electric potential gradient. Additionally ϕ is set to 0 at the upper right corner of the domain.

The simulation conditions are described now. The chamber has a length of $L = 4cm$ and a radius of $R = 1cm$. Xenon is injected uniformly at the back of the chamber; the mass flow is $\dot{m} = 0.1mg/s$, and the injection axial velocity and temperature are $u_n^{inj} = 300m/s$ and $T_n^{inj} = 0.02eV$. The (constant) electron temperature is $T_e = 8eV$.

The topology and strength of the applied magnetic field is shown in Fig. 3(a). It presents a singularity ($B = 0$) at the axis. Although near axial magnetic fields are used in conventional HPT designs, we have selected this case on purpose to illustrate the capabilities of the code. Figure 3(b) shows in red the resulting magnetic mesh, made of magnetic streamlines and the orthogonal to them. Observe the disparity in sizes and forms of the cells, which makes challenging an accurate integration of electron equations. Superimposed in black it is the rectangular mesh used by the I-module. Interpolation between meshes is another source of potential error. The I-module mesh uniform resolution considers 10 intervals in the radial direction and 40 in the axial one.

The I-module timestep is 50 nanoseconds. Ions impinging the walls are recombined; an accommodation factor of $\alpha_w = 0.7$ and a wall temperature of $T_w = 0.02$eV are used. Neutrals impinging the walls are reflected diffusively. A forcing algorithm is applied at the lateral walls so that the electric potential profile and the ion flow satisfy the Bohm condition at the quasineutral boundary [16]. The simulations are run until $1.5ms$, when a stationary discharge is well established.
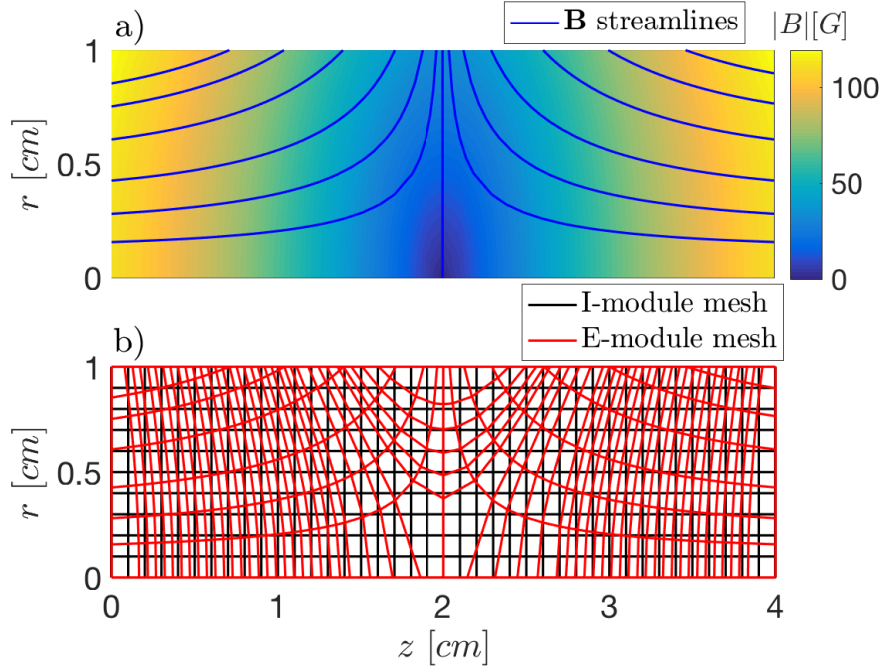
Figure 3: (a) Magnetic field topology: strength and streamlines. (b) Ortoghonal meshes used by the I-module (black) and the E-module (red).

4. RESULTS

Results obtained for the simulation case defined above are presented in Figs. 4 to 5. References values for velocities, densities, and current densities are $c_s = \sqrt{T_e/m_i} = 2.42$ km/s, $n_0 = \dot{m}/(\pi R^2 m_i c_s) = 6 \cdot 10^{17}$m^{-3} and $j_0 = en_0c_s = 23.2$mA/cm^2 with m_i is the ion mass.
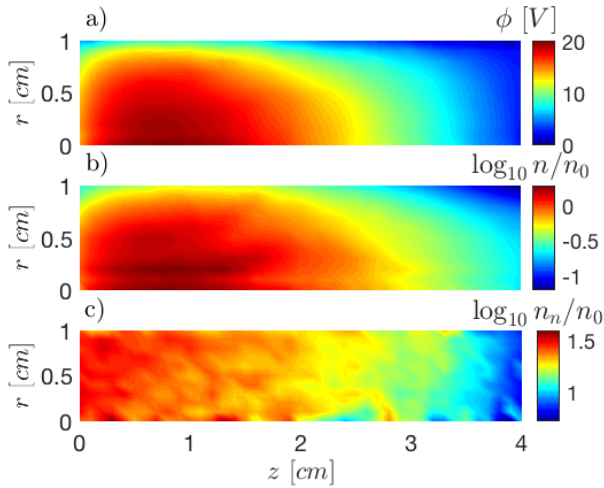

Figure 4: Results for (a) the electric potential, (b) the plasma density, and (c) the neutral density.

Profiles of the electric potential, plasma density and neutral density are shown in Fig. 4. Plasma production takes place mainly in the back half-region of the channel. Later ionization is mainly due to wall recombination. This also makes that the neutral density map has a marked a 2D character. The maxi-

mum of plasma density is thus placed in the same back-region and near the axis. Axial and radial ion acceleration (from Fig. 5) further explain the map of plasma density in the front half-region and near the lateral walls. The profile of the electric potential follows approximately the logarithm of the density, indicating that the Boltzmann relation is satisfied approximately. The total potential fall in this simplified, uncompleted plasma expansion is about 2.5 times the temperature
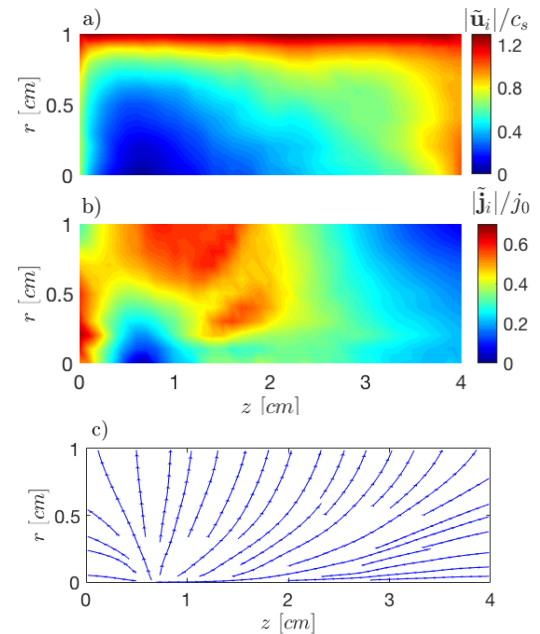

Figure 5: Longitudinal ion velocity at (a), current density at (b) and direction at (c).

The ion velocity and current density are displayed at Fig. 5, both magnitudes and direction. The vectors $\tilde{\mathbf{u}}_i$ and $\tilde{\mathbf{j}}_i$ contain only the longitudinal components, i.e. axial and radial ones. We observe that the point of zero current is close to the points of maximum potential and density as it must be. From there, the ion fluid is accelerated towards every direction and not just to the exit. Furthermore, the ion current recombined at the back half-region is the largest one. All this implies a low production efficiency (i.e. the ratio between the ion current in the externally emitted beam and the total ion current to all surfaces). One reason is that the present magnetic topology, although convenient for illustrating the code capabilities, does not seem adequate for a good thruster design.

Fig. 6 plots the electron current density maps. It is convenient to separate the current density vector into its azimuthal and longitudinal components, $\mathbf{j_e} = \tilde{\mathbf{j}}_e + j_{\theta e}\mathbf{1}_\theta$. The same division can be applied to the ions but the ion azimuthal density is negligible. The applied magnetic field yields a Hall parameter of up to $\beta_e \sim 100$, which is already high enough to generate large azimuthal currents, as seen in panel (c). There is a change in the sign of $j_{\theta e}$ from the back side of the chamber to the front side marked by the blue line due to the opposite direction of $\mathbf{B}$ at each side of the singular point. The pattern of the longitudinal electron current density, $\tilde{\mathbf{j}}_e$, is different from the one for the ions: it is governed by the topology of the magnetic field (which tends to align $\tilde{\mathbf{j}}_e$) and the boundary conditions at the walls (which do depend on the ion current density).
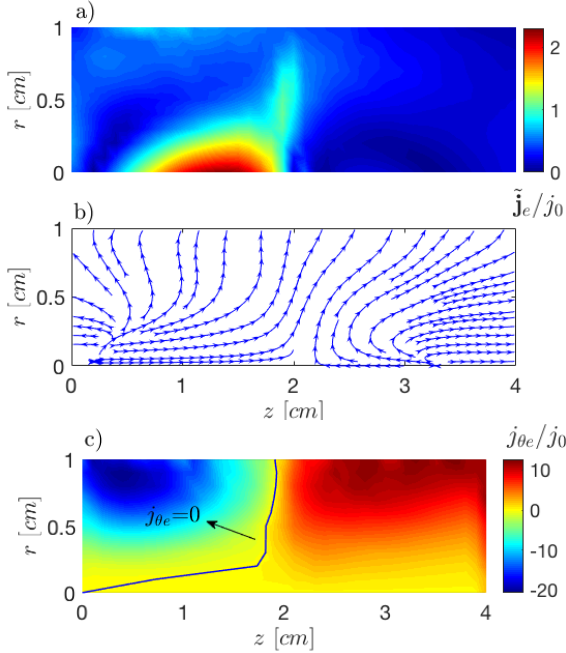
Fig. 7 shows the longitudinal electric current density, obtained by adding the ion and electron contributions. Since the chamber walls are dielectric, $\tilde{\mathbf{j}}$ is aligned with the chamber walls. The magnitude of the net electric current indicates that 'current ambipolarity' (i.e. $\tilde{\mathbf{j}}$), assumed in [13], is not satisfied, although the deviations are located only in parts of the back region. This contrasts with the approximate symmetry of the lines with respect to the mid chamber section. Interestingly, at the chamber exit the total net current is zero but the net current density is outwards near the axis (dominated by ions) and backwards (dominated by electrons) near the chamber wall. A similar behavior has been found in simulations with magnetic nozzles [17].
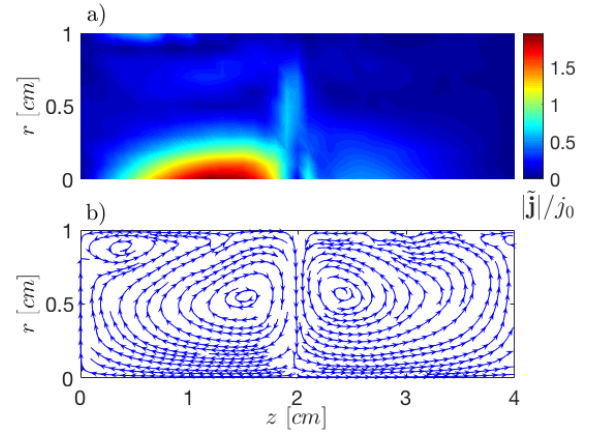

Figure 7: Longitudinal electric current density: (a) strength, (b) direction.

5. CONCLUSIONS

The preliminary version of a 2D hybrid code has proved to simulate the plasma transport in a HPT configuration with a complex magnetic topology. The results obtained from the simulation case have allowed to provide a first idea of the plasma dynamics inside a HPT chamber. Work in progress includes the simulation of the plasma expansion along the external magnetic nozzle and the determination of thruster performances.

Figure 6: Electron current density: (a) and (b) longitudinal current strength and direction, respectively; (c) azimuthal current.

REFERENCES

[1] Ahedo, E., "Plasma dynamics in a helicon thruster," *Proceedings of EUCASS 2011, Saint Petersburg, Russia*, 2011.

[2] Pavarin, D. et al., "Design of 50W Helicon Plasma Thruster," *31th International Electric Propulsion Conference, Ann Arbor, Michigan, US*, 2009.

[3] Ziemba, T., Euripides, P., Slough, J., Winglee, R., Giersch, L., Carscadden, J., Schnackenberg, T., and Isley, S., "Plasma characteristics of a high power helicon discharge," *Plasma Sources Science and Technology*, Vol. 15, No. 3, 2006.

[4] West, M., Charles, C., and Boswell, R., "Testing a Helicon Double Layer Thruster immersed in a space-simulation chamber," *Journal of Propulsion and Power*, Vol. 24, No. 1, 2008, pp. 134–141.

[5] Takahashi, K., Charles, C., Boswell, R., and Ando, A., "Performance improvement of a permanent magnet helicon plasma thruster," *Journal of Physics D: Applied Physics*, Vol. 46, No. 35, 2013.

[6] Navarro, J., Wijnen, M., Fajardo, P., and Ahedo, E., "Experimental characterization of a 1kW Helicon Plasma Thruster," *Vacuum*, Vol. 149, 2018, pp. 69–73.

[7] Shamrai, K. and Taranov, V., "Resonance wave discharge and collisional energy absorption in helicon plasma source," *Plasma Physics and Controlled Fusion*, Vol. 36, 1994, pp. 1719–1735.

[8] Cho, S. and Lieberman, M., "Self-consistent discharge characteristics of collisional helicon plasmas," *Physics of Plasmas*, Vol. 10, 2003, pp. 882–890.

[9] Tian, B., Ahedo, E., and Merino, M., "Development and validation of a 2D wave-plasma code for Helicon Plasma Thrusters," *Space Propulsion Conference 2016, Rome, Italy*, 2016.

[10] Navarro, J., Wijnen, M., Fajardo, P., Merino, M., Ahedo, E., Gómez, V., and Ruiz, M., "Experimental performances of a 1kW HPT by means of plasma diagnostics," *35th International Electric Propulsion Conference, Atlanta, Georgia, US*, 2017.

[11] Pérez-Grande, D., Zhou, J., Domínguez, A., Fajardo, P., and Ahedo, E., "Development updates for a two-dimensional axisymmetric hybrid code for plasma thruster discharges," *35th International Electric Propulsion Conference, Atlanta, Georgia, US*, 2017.

[12] Domínguez, A., Pérez-Grande, D., Fajardo, P., and Ahedo, E., "NOMADS: Development of a versatile plasma discharge simulation platform for electric propulsion," *Space Propulsion Conference 2016, Rome, Italy*, 2016.

[13] Ahedo, E. and Navarro, J., "Helicon thruster plasma modeling: Two-dimensional fluid-dynamics and propulsive performances," *Physics of Plasmas*, Vol. 20, No. 4, 2013.

[14] Sánchez-Villar, A., Merino, M., and Ahedo, E., "Advances in wave-plasma modelling in ECR thrusters," *Space Propulsion Conference 2018, Seville, Spain*, 2018.

[15] Pérez-Grande, D., González-Martínez, O., Fajardo, P., and Ahedo, E., "Analysis of the numerical diffusion in anisotropic mediums: Benchmarks for magnetic field aligned meshes in space propulsion simulations," *Applied Sciences*, Vol. 6, No. 11, 2016.

[16] Ahedo, E., Santos, R., and Parra, F., "Fulfilment of the kinetic Bohm criterion in a quasineutral particle-in-cell model," *Physics of Plasmas*, Vol. 17, 2010, pp. 073507.

[17] Ahedo, E. and Merino, M., "Two-dimensional supersonic plasma acceleration in a magnetic nozzle," *Physics of Plasmas*, Vol. 17, No. 7, 2010.